Inverse Dopant Profiling from Transient Measurements

M.-T. Wolfram*

Abstract

In this work we investigate inverse problems related to the transient semiconductor device models. Our main focus is the identification of the doping profile from indirect transient measurements of electrical currents and capacitances. We present the underlying analysis and discuss the applied regularization methods. Furthermore we discuss the identifiability of doping profiles and present uniqueness and non-uniqueness results for regularized solutions.

1 Introduction

The first fundamental semiconductor device model, called the drift-diffusion equations was introduced by Van Roosbroeck [1] in 1950. Today different models of various complexity exist, but the drift-diffusion equations seem to be a good compromise between efficiency and accurate description of the underlying device physics. For detailed information on the derivation of semiconductor device models and the corresponding analysis we refer to [2] and [3].
Nowadays industry is strongly interested in the identification of doping profiles for quality control purposes. Furthermore there has been a growing demand on optimizing the performance of semiconductor devices. For identification problems destructive tests, like spreading resistance profiling or non-destructive techniques, such as current, capacitance and or laser-beam-inducted current (LBIC) measurements, are used.
Identification and optimal design problems using current or capacitance measurements have been investigated concerning steady state models. There has been recent work on optimizing the performance of devices (see e.g. [4],[5]) and in identifying relevant material properties (see e.g. [6],[7],[8]). The inverse problem of reconstructing the doping profile from LBIC measurements has been considered in [8] and [9].
The main focus of this paper is the identification of the doping profile from indirect transient measurements. In steady state models current and capacitance measurements are taken for several applied voltages in equilibrium. In case of the transient model several measurements, taken at different time steps, are available for a single applied voltage. An additional advantage is the simpler mathematical analysis. Uniqueness results for the forward stationary problem require a smoothness and smallness condition on the applied voltage, while this

*This work has been supported by the Austrian National Science Foundation (FWF) through project SFB F013/P1308

is not necessary for the transient model (see [10]). Furthermore the identification problem for simplified semiconductor devices has a unique solution in the one-dimensional setup (see [6]). These advantages motivate the use of time dependent models for the reconstruction of the doping profile, although it is not always possible to obtain reliable transient measurements.
The transient drift-diffusion model is a system of nonlinear partial differential equations and requires consistent initial values. In practice it is assumed that a semiconductor device is at thermal equilibrium at $t = 0$. Therefore we use the equilibrium solution as initial value for the transient problem. In this context we discuss inverse problems related to the different measurement techniques.
The paper is organized as follows. In section 2 we introduce the transient drift-diffusion equations and discuss the underlying analysis briefly. The inverse problem of reconstructing the doping profile from indirect measurements is presented in section 3. Furthermore the adjoint approach, used for gradient evaluation is introduced shortly in section 4. The identifiability of the doping profile from indirect measurements is discussed in section 5. Finally we present solutions of computational examples in section 6.

2 The Transient Drift-Diffusion Equations

The drift-diffusion model stated on a bounded domain $\Omega \subset \mathbb{R}^d, d = 1, 2, 3$ reads as

$$\begin{aligned} \operatorname{div}(\epsilon \nabla V) &= q(n - p - C) \\ \operatorname{div} J_n &= q\left(\partial_t n + R\right) \\ \operatorname{div} J_p &= q\left(-\partial_t p - R\right) \\ J_n &= q\left(D_n \nabla n - \mu_n n \nabla V\right) \\ J_p &= q\left(-D_p \nabla p - \mu_p p \nabla V\right). \end{aligned} \tag{1}$$

The variables are

- the electrical potential V
- and the concentrations electrons n and holes p.

The predefined doping profile is donted by $C = C(x)$ and the total current density is given by $J = J_n + J_p$. The parameters D_n, D_p, μ_n, and μ_p are the diffusion coefficients and mobilities of electrons and holes respectively. In general they can be modelled by positive functions, in the following they are assumed to be constant. Here ϵ and q are the permittivity constant and the elementary charge.
The function R is the recombination-generation rate. Several models can be found in literature, we consider the Shockley-Read-Hall (SRH) recombination-generation rate

$$R_{SRH} = \frac{np - n_i^2}{\tau_p(n + n_i) + \tau_n(p + n_i)}$$

where n_i denotes the intrinsic density and τ_n and τ_p are the lifetime of the electrons and holes respectively.

We assume that the boundary of the semiconductor is divided into two parts. On the Dirichlet part $\partial\Omega_D$ the boundary conditions

$$n(x,t) = n_D(x), \quad p(x,t) = p_D(x)$$
$$V(x,t) = U(x,t) + U_T \ln \frac{n_D(x)}{n_i},$$

hold, on the Neumann part $\partial\Omega_N$, modeling insulation, the conditions

$$\frac{\partial V}{\partial \nu} = 0 \qquad J_n(x,t)\cdot\nu = 0 \qquad J_p(x,t)\cdot\nu = 0.$$

are satisfied. Here U_T is the thermal voltage and $U(x,t)$ denotes the applied potential on $\Gamma_D \subset \partial\Omega_D$. Initial conditions for the free carrier concentrations n and p at the time $t = 0$ are given by

$$n(x,0) = n^I(x) \qquad p(x,0) = p^I(x) \qquad x \in \Omega.$$

We apply a suitable scaling to (1) (cf. [3]) and obtain the dimensionless formulation of the drift-diffusion equations

$$\begin{aligned} \lambda^2 \triangle V &= n - p - C \\ \partial_t n &= \operatorname{div} J_n - R \\ \partial_t p &= -\operatorname{div} J_p - R \\ J_n &= \mu_n (\nabla n - n \nabla V) \\ J_p &= \mu_p (-\nabla p - p \nabla V) \end{aligned} \tag{2}$$

with the appropriate scaled boundary conditions.
The parameter

$$\lambda = \left(\frac{\varepsilon U_T}{q\tilde{C}L^2}\right)^{\frac{1}{2}}$$

is called scaled Debye length. (The Debye length is the quantity $\sqrt{\varepsilon U_T/q\tilde{C}} = \lambda L$.) The parameters L and $\tilde{C}$ are the characteristic length and the maximal absolute value of the doping concentration respectively, which satisfy $x = Lx_s$ and $C = \tilde{C}C_s$. The scaled variables are then dimensionless and at most of order $O(1)$. For small devices and highly doped semiconductors λ tends to zero acting as a singular perturbation parameter.

2.1 The Equilibrium Case

A semiconductor device is in thermal equilibrium, if $U(x) \equiv 0$ and $R \equiv 0$, i.e. no potentials are applied to the semiconductor contacts and the thermal generation is exactly balanced by recombination.
Solutions of the reduced stationary drift-diffusion equations

$$\begin{aligned} \lambda^2 \Delta V &= n - p - C \\ 0 &= \mu_n (\nabla n - n \nabla V) \\ 0 &= \mu_p (\nabla p - p \nabla V) \end{aligned}$$

are then given by

$$n = \sigma^2 e^V \qquad\qquad p = \sigma^2 e^{-V}. \tag{3}$$

The system then reduces to a nonlinear Poisson equation

$$\lambda^2 \Delta V = \sigma^2 e^V - \sigma^2 e^{-V} - C \tag{4}$$

for the potential V with the boundary conditions

$$\begin{aligned} V(x) = V_{bi}(x) = \ln\,(\frac{1}{2\sigma^2}(C(x) + \sqrt{C(x)^2 + 4\ \sigma^4}) \qquad & \forall x \in \partial\Omega_D \\ \frac{\partial V}{\partial \nu} = 0 \qquad & \forall x \in \partial\Omega_N. \end{aligned}$$

In practice it is assumed that the process starts around equilibrium. Therefore n_0 and p_0 given by (3), with V_0 obtained by solving the Poisson equation (4), can be used as initial values for the time-dependent problem (2).

2.2 Analysis of the Transient Drift-Diffusion Model

In this section we discuss existence and uniqueness results for the transient drift-diffusion model and specialize them to the one-dimensional case.
In [10] existence and uniqueness of global-in-time solutions for the transient drift-diffusion equations is proven. Let d denoted the space dimension and $d \leq r \leq 6$. Then under the assumption that the doping profile satisfies $C \in L^r(\Omega)$ it is shown that $(V - V_D, n - n_D, p - p_D) \in W$ where W is defined as follows:

$$W = \left\{C([0,T]; W^2_{2,0}) \cap L^2([0,T]; W^2_{r,0}) \cap H^1([0,T]; X)\right\} \times Y \times Y,$$

with

$$\begin{aligned} Y &= C([0,T]; L^2) \cap L^2([0,T], X) \cap H^1([0,T], X^*) \\ X &= \left\{v \in W^1_2 \mid v = 0 \text{ on } \partial\Omega_D\right\}. \end{aligned}$$

We consider the following assumptions:

(A1) $\Omega = [0,1]$;

(A2) The doping profile satisfies $C \in L^r(\Omega)$;

(A3) The mobilities satisfy $\mu_n \in L^\infty(\Omega), \mu_p \in L^\infty(\Omega)$;

(A4) The recombination-generation rate satisfies $R \in C([0,T], L^2(\Omega))$.

Note that assumption (A4) for the RSH recombination-generation rate is satisfied if $\tau_n, \tau_p \in L^\infty(\Omega)$. For the special case of spatial dimension one we are able to show higher regularity of (V, n, p).

Proposition 2.1. *Under the assumptions (A1)-(A4) stated above every solution* $(V - V_D, n - n_D, p - p_D) \in W$ *satisfies* $(V, n, p) \in \tilde{W}$ *where* $\tilde{W}$ *is defined as follows:* $\tilde{W} = C([0,T], H^2(\Omega)) \times C([0,T], W^1_\infty(\Omega))^2$.

For the proof of Proposition 2.1 we refer to [11]. Furthermore in [12] it has been proven that the linearization of the drift-diffusion equations is a strongly continuous semigroup and invertible.

3 Identification of the doping profile

Inverse dopant profiling corresponds to the identification of the doping profile $C(x)$ in system (2) from indirect measurements. The authors are conscious of the fact that capacitance-voltage measurements are most commonly used in practice, but for small-geometry devices with very small capacitances voltage-current measurements proved to be a useful alternative (see e.g. [13]). The following types of measurements are used in practice:

1) *Current measurements:*
The current flow through a contact $\Gamma_1 \subset \partial\Omega_D$ is given by

$$\mathcal{I}_{\Gamma_1}(U) = \int_{\Gamma_1} (J_n + J_p) \cdot \nu \, ds. \tag{5}$$

2) *Capacitance measurements:*
The mean capacitance at a contact $\Gamma_1 \subset \partial\Omega_D$ is given by

$$\mathcal{C}_{\Gamma_1}(U) = \frac{d}{dU} \left(\int_{\Gamma_1} \frac{\partial V}{\partial \nu} \, ds \right). \tag{6}$$

Note that for $\Gamma_1 = \partial\Omega$

$$\mathcal{C}(U) = \frac{d}{dU} \left(\int_{\partial\Omega} \frac{\partial V}{\partial \nu} ds \right) = \frac{d}{dU} \left(\int_{\Omega} \Delta V dx \right) = \frac{d}{dU} Q,$$

where Q denotes the total space charge.
Considering both type of measurements we assume that $\Gamma_1 \subset \partial\Omega_D$ is sufficiently regular with non zero measure. A second contact is denoted by $\Gamma_2 \subset \partial\Omega_D$ with $\Gamma_1 \cap \Gamma_2 = \emptyset$.
In the following we investigate whether the operators, mapping the applied potential U on Γ_2 to the current or capacitance measurements, are well-defined and continuous between appropriate spaces.

The Current-Voltage Map

The voltage current data are the measurements of the normal component of the current density J on a contact $\Gamma_1 \subset \partial\Omega_D$ for an applied time dependent voltage $U(x,t)$. The current-voltage map is given by:

$$\begin{aligned} \Sigma_C : L^2([0,T], H^{\frac{1}{2}}(\Gamma_2)) &\to L^2([0,T]) \\ U &\mapsto \mathcal{I}_{\Gamma_1}(U) \end{aligned} \tag{7}$$

In [11] we proof the following proposition

Proposition 3.1. *The nonlinear operator Σ_C defined by (7) is well-defined, continuous and Fréchet-differentiable.*

Capacitance Measurements

Capacitance measurements are the variation of the electric flux in normal direction on a contact Γ_1 with $U = 0$ with respect to the applied voltage U on Γ_2.

The corresponding operator is given by

$$T_C : L^2([0,T], H^{\frac{1}{2}}(\Gamma_2)) \to L^2([0,T])$$
$$\phi \mapsto \int_{\Gamma_1} \frac{\partial \hat{V}}{\partial \nu}\, ds$$

where $\hat{V}$ is the solution of the linearized drift-diffusion equations around equilibrium, i.e.

$$\begin{aligned} \lambda^2 \Delta \hat{V} &= \hat{n} - \hat{p} \\ \frac{\partial \hat{n}}{\partial t} &= \operatorname{div}\left(\mu_n \left(\nabla \hat{n} - \sigma^2\ e^{V_0}\ \nabla \hat{V} - \hat{n}\ \nabla V_0\right)\right) \\ \frac{\partial \hat{p}}{\partial t} &= \operatorname{div}\left(\mu_p \left(\nabla \hat{p} + \sigma^2\ e^{-V_0}\ \nabla \hat{V} + \hat{p}\ \nabla V_0\right)\right) \end{aligned} \tag{8}$$

with homogeneous initial conditions, homogeneous Neumann boundary conditions and the Dirichlet boundary conditions on $\partial\Omega_D$

$$\hat{V} = \phi, \quad \hat{n} = \hat{p} = 0.$$

Here V_0 denotes the solution of the Poisson equation in thermal equilibrium calculated via (4). We can show that the nonlinear operator T_C is well-defined, continuous and Fréchet-differentiable between suitable Sobolev spaces, see [11]. In the next sections we discuss the identification of the doping profile from either current or capacitance measurements.

3.1 Identification from Voltage-Current Data

The abstract formulation of the identification problem using current measurements is given by

$$F(C) = Y^\delta \tag{9}$$

with

$$F\colon D(F) \subset \mathcal{X} \mapsto \mathcal{Y}$$
$$C \mapsto \Sigma_C(U)$$

and $\mathcal{X} = L^2(\Omega),\ \mathcal{Y} = L^2([0,T])$. The domain of the operator F is restricted to

$$D(F) = \left\{C \in H^1(\Omega) \mid \underline{C} \le C(x) \le \overline{C} \text{ a.e. in } \Omega\right\}$$

with positive constants $\underline{C}$ and $\overline{C}$.
Y^δ represents the noisy current data bounded by δ, i.e.

$$\left\|Y^\delta - Y\right\| \le \delta. \tag{10}$$

Under these assumptions we are able to verify the following result.

Proposition 3.2. *The map*

$$F\colon D(F) \subset \mathcal{X} \to \mathcal{Y}$$
$$C \mapsto \Sigma_C(U)$$

is well-defined, continuous and Fréchet-differentiable. Furthermore the operator F is weakly sequentially closed, i.e. for any sequence $\{C_n\} \subset D(F)$, weak convergence of C_n to $C \in \mathcal{X}$ and weak convergence of $F(C_n)$ to $y \in \mathcal{Y}$ imply that $C \in D(F)$ and $F(C) = y$.

The main idea of the proof is to rewrite the operator F as

$$\begin{aligned} F &= F_1 \circ F_2 \\ F_2 &: C \to (n, p, V) \\ F_1 &: (n, p, V) \to J \cdot \nu \end{aligned}$$

and to show that both operators are continuous and Fréchet differentiable. For further information on the proof we refer to [11].

3.2 Identification from Capacitance Measurements

Similar to the case of current-voltage data the identification problem can be written in the abstract form

$$F(C) = Y^\delta \tag{11}$$

with

$$F\colon D(F) \subset \mathcal{X} \mapsto \mathcal{Y} \tag{12}$$

$$C \mapsto T_C(U) \tag{13}$$

and $\mathcal{X} = L^2(\Omega), \mathcal{Y} = L^2([0,T])$. The domain of the operator F is the same as in the case of the voltage-current map.

Proposition 3.3. *The map*

$$\begin{aligned} F\colon D(F) \subset \mathcal{X} &\to \mathcal{Y} \\ C &\mapsto T_C(U) \end{aligned}$$

is well-defined, continuous and Fréchet-differentiable in $\mathcal{X}$. Furthermore the operator F is weakly sequentially closed.

The proof uses similar arguments as in case of current measurements, again we refer to [11] for details.

3.3 Regularization Methods

The problem of solving (9) or (11) is ill-posed. In the sense of Hadamard this means that a solution might not exist nor be unique or depend continuously on the data. Because of the ill-posedness and the noise in the data caused by measurement errors, standard iterative methods cannot be used to solve (9) or (11) in a stable way. Therefore we use special techniques, so called regularization methods, to obtain a stable solution. In this section we discuss regularization methods which we use for the numerical simulations in section 6. For further information on inverse problems and regularization methods we refer to [14, 15].

The prerequisite (10) on the noisy data in case of current measurements is given by

$$\int_0^T \left|\mathcal{I}(t) - i^\delta(t)\right|^2 \, dt \leq \delta^2, \tag{14}$$

where $i^\delta(t)$ denotes the current measured on $\Gamma_1 \subset \partial\Omega_D$. For capacitance measurements we have

$$\int_0^T \left|\mathcal{C}(t) - c^\delta(t)\right|^2 \, dt \leq \delta^2, \tag{15}$$

where $c^\delta(t)$ is the capacitance measured on $\Gamma_1 \subset \partial\Omega_D$.

Tikhonov Regularization

A standard regularization method for nonlinear problems is the Tikhonov regularization. Using Tikhonov regularization, equation (9) is replaced by the minimization problem

$$\left\|F(C) - Y^\delta\right\|^2_{L^2([0,T])} + \alpha \left\|C - C^*\right\|^2_{L^2(\Omega)} \to \min_{C \in D(F)}, \tag{16}$$

where $\alpha > 0$. The function C^* denotes some initial guess, which incorporates a-priori knowledge of the solution. If the solution is not unique the second term will favor a solution with minimal distance to C^*. We refer to α as the regularization parameter, which is determined by the Morozov's discrepancy principle, i.e. the largest α such that

$$\left\|F\left(C_\alpha^\delta\right) - Y^\delta\right\|_{L^2([0,T])} = \delta, \tag{17}$$

is satisfied. Here C_α^δ denotes the regularized solution, which depends on the regularization parameter α and on the noise level δ.
A regularized solution C_α^δ is the global minimizer of the Tikhonov functional (16). The Tikhonov functional is not convex for nonlinear problems and might have local minima. This fact is the underlying cause of the numerical problems which we will discuss in section 5. Since F is continuous and weakly sequentially closed we are able to verify the following result.

Proposition 3.4. *The minimization functional (16) admits a solution C, if F is continuous and weakly sequentially closed. Furthermore the problem has a stable dependence on the perturbed data Y^δ, i.e. if δ tends to zero the regularized solution converges to the exact solution.*

For detailed information on the proof we refer to [11], for the convergence analysis to [14].

Total Variation Regularization

This Tikhonov-type regularization method uses the total variation of a function. Total variation regularization, introduced in [16], was originally used in image restoration, because it preserved discontinuities in the solution. Because of the jump of the doping profile at the pn-junction this approach is interesting. For further information on the underlying analysis we refer to [17, 18].
The total variation functional is defined by:

$$J_0(u) := \sup_{v \in V} \int_\Omega u \operatorname{div} v \, dx,$$

where the set of test functions is given by

$$V = \left\{ v \in C_0^\infty(\Omega)^d \mid \|g\|_\infty \leq 1 \right\}.$$

If $u \in C^1(\Omega)$ one can show, using integration by parts that

$$J_0(u) = \int_\Omega |\nabla u| \, dx \tag{18}$$

The seminorm (18) is not differentiable where $\nabla u = 0$ therefore one often considers the slightly modified functional

$$J_\beta(u) = \int_\Omega \sqrt{|\nabla u|^2 + \beta} \, dx$$

with $\beta \geq 0$. The corresponding regularized minimization problem is given by

$$\left\| F(C) - Y^\delta \right\|^2 + \alpha J_\beta(C) \to \min_{C \in D(F)}, \tag{19}$$

where α denotes the regularization parameter, determined by the discrepancy principle (17).
In [18] it is shown that a solution of the minimization problem (19) exists, if Q is weakly lower semicontinuous and BV-coercive. For both current and capacitance measurements we are able to verify the properties in an analogous to Tikhonov regularization.

4 Sensitivities

For either type of regularization method one has to solve a constrained minimization problem which can be written as

$$Q(u(C), C) \to \min_C \quad \text{subject to} \quad P(u(C), C) = 0.$$

The restriction $P(u(C), C) = 0$ is the transient drift-diffusion system (2) and the system in thermal equilibrium (4) with $u = (V, V_0, n, p)$.
In the previous section we proved that for either regularization method a minimizer exists and that all operators are continuous and Fréchet differentiable. Therefore one can use gradient based methods for minimization. The total derivative of the minimization problem can be calculated via the corresponding Lagrange functional using the adjoint equations. The Lagrange functional $\mathcal{L}$ is given by

$$\mathcal{L}(u, C, \lambda) = Q(u, C) + \langle P(u, C), \lambda \rangle.$$

With the Kuhn Tucker restrictions

$$\frac{\partial \mathcal{L}}{\partial u}(u, C, \lambda) = \frac{\partial Q}{\partial u}(u, C) + \frac{\partial P}{\partial u}^*(u, C)\ \lambda = 0 \tag{20}$$

$$\frac{\partial \mathcal{L}}{\partial C}(u, C, \lambda) = \frac{\partial Q}{\partial C}(u, C) + \frac{\partial P}{\partial C}^*(u, C)\ \lambda = 0 \tag{21}$$

$$\frac{\partial \mathcal{L}}{\partial \lambda}(u, C, \lambda) = P(u, C) = 0 \tag{22}$$

the Lagrange parameter λ can be calculated using (20). By the chain rule the linearization of Q is given by

$$\frac{dQ}{dC} = \frac{\partial Q}{\partial u}\frac{du}{dC} + \frac{\partial Q}{\partial C} \tag{23}$$

subject to the constraint that du/dC solves the linearized equation

$$\frac{\partial P}{\partial C}\frac{du}{dC} + \frac{\partial P}{\partial C} = 0.$$

Then inserting λ into (21) and rearranging (23) yields to

$$\frac{dQ}{dC}h = \frac{\partial \mathcal{L}}{\partial C}h \quad \forall h \in L^2(\Omega).$$

Hence, the total derivative $\frac{dQ}{dC}$ can be calculated using the Fréchet derivative of the corresponding Lagrange functional $\mathcal{L}$ with respect to C. For detailed information on the adjoint approach we refer to [19].
For solving (16) or (19) we use a projected steepest descent algorithm or a projected BFGS method (see [20] or [21]). In case of n-type semiconductors the additional constraint $C(x) \geq 0$ has to be satisfied.

Current Measurements

The adjoint system in case of current measurements and Tikhonov regularization is given by

$$\begin{aligned} -\lambda_1 - \frac{\partial \lambda_2}{\partial t} - \mu_n\ \Delta\lambda_2 - \mu_n\ \nabla V\ \nabla\lambda_2 + (\lambda_2 + \lambda_3)\frac{\partial R}{\partial n} &= 0 \\ \lambda_1 - \frac{\partial \lambda_3}{\partial t} - \mu_p\ \Delta\lambda_3 + \mu_p\ \nabla V\ \nabla\lambda_3 + (\lambda_2 + \lambda_3)\frac{\partial R}{\partial p} &= 0 \\ \lambda^2 \Delta\lambda_1 + \mu_n\ \operatorname{div}(n\ \nabla\lambda_2) - \mu_p\ \operatorname{div}(p\ \nabla\lambda_3) &= 0 \end{aligned} \tag{24a}$$

in $\Omega \times [0,T]$ and

$$\lambda^2\ \Delta\lambda_4 - \sigma^2\ \lambda_4\ (e^{V_0} + e^{-V_0}) = \sigma^2\ (\lambda_2(\cdot,0)\ e^{V_0} - \lambda_3(\cdot,0)\ e^{-V_0}) \tag{24b}$$

in $\Omega \times \{0\}$. The Dirichlet boundary conditions are

$$\begin{aligned} \lambda_2 &= \int_{\partial\Omega} \left[\mu_n(\nabla n - n\nabla V) - \mu_p(\nabla p + p\ \nabla V)\right]\nu\ ds - i^\delta(t) && \text{on } \Gamma_1 \times [0,T] \\ \lambda_3 &= -\int_{\partial\Omega} \left[\mu_n(\nabla n - n\nabla V) - \mu_p(\nabla p + p\ \nabla V)\right]\nu\ ds + i^\delta(t) && \text{on } \Gamma_1 \times [0,T] \end{aligned}$$

$$\begin{aligned} \lambda_2 &= 0 && \text{on } \Gamma_2 \times [0,T] \\ \lambda_3 &= 0 && \text{on } \Gamma_2 \times [0,T] \\ \lambda_1 &= 0 && \text{on } \partial\Omega_D \times [0,T] \\ \lambda_4 &= 0 && \text{on } \partial\Omega_D. \end{aligned}$$

Furthermore we have homogeneous Neumann boundary conditions and the terminal conditions are given by:

$$\lambda_2(x,T) = \lambda_3(x,T) = 0 \qquad \forall x \in \Omega.$$

The partial derivative of the Lagrange functional in case of Tikhonov regularization (16) is given by

$$\frac{\partial \mathcal{L}}{\partial C}\ h_C = \int_0^T \int_\Omega \lambda_1\ h_C\ dx\ dt + \int_\Omega \lambda_4\ h_C\ dx + \alpha \int_\Omega |C - C^*|\ h_C\ dx. \tag{25}$$

Capacitance Measurements

In case of capacitance measurements the adjoint system is given by

$$\begin{aligned} \lambda^2\ \Delta\lambda_1 + \mu_n\ \sigma^2 \operatorname{div}\left(e^{V_0}\ \nabla\lambda_2\right) - \mu_p\ \sigma^2 \operatorname{div}\left(e^{-V_0}\ \nabla\lambda_2\right) &= 0 \\ -\lambda_1 - \frac{\partial \lambda_2}{\partial t} - \mu_n\ \Delta\lambda_2 - \mu_n\ \nabla V_0\ \nabla\lambda_2 &= 0 \\ \lambda_1 - \frac{\partial \lambda_3}{\partial t} - \mu_p\ \Delta\lambda_3 + \mu_p\ \nabla V_0\ \nabla\lambda_3 &= 0 \end{aligned} \tag{26a}$$

and in $\Omega \times \{0\}$

$$\begin{aligned} &\lambda^2 \Delta\lambda_4 - \sigma^2\ e^{V_0}\lambda_4 - \sigma^2\ e^{-V_0}\lambda_4 = \\ &\int_0^T \left(-\operatorname{div}\left(\mu_n\ \hat{n}\ \nabla\lambda_2\right) + \sigma^2\ e^{V_0}\ \nabla\hat{V}\ \nabla\lambda_2\right) dt + \\ &+ \int_0^T \left(\operatorname{div}\left(\mu_p\ \hat{p}\ \nabla\lambda_3\right) + \sigma^2\ e^{-V_0}\ \nabla\hat{V}\ \nabla\lambda_3\right) dt + \\ &+ \lambda_2(x,0)\ \sigma^2\ e^{V_0}\ \hat{V}(x,0) - \lambda_3(x,0)\ \sigma^2\ e^{-V_0}\ \hat{V}(x,0). \end{aligned} \tag{26b}$$

The corresponding Dirichlet boundary conditions on $\partial\Omega_D = \Gamma_1 \cup \Gamma_2$,with $\Gamma_1 \cap \Gamma_2 = \emptyset$ are

$$\begin{aligned} \lambda_1 &= -\frac{1}{\lambda^2}\left(\frac{\partial \hat{V}}{\partial \nu} - c^\delta(t)\right) && \text{on } \Gamma_1 \times [0,T] \\ \lambda_1 &= 0 && \text{on } \Gamma_2 \times [0,T] \\ \lambda_2 &= 0 && \text{on } \partial\Omega_D \times [0,T] \\ \lambda_3 &= 0 && \text{on } \partial\Omega_D \times [0,T] \\ \lambda_4 &= 0 && \text{on } \partial\Omega_D \end{aligned}$$

On the rest of the boundary we have homogeneous Neumann boundary conditions. Again we obtain homogenous terminal conditions for λ_2 and λ_3 instead of initial conditions. The partial derivative of the corresponding Lagrange functional with respect to C is given by

$$\frac{\partial \mathcal{L}}{\partial C}\ h_C = \int_\Omega \lambda_4\ h_C\ dx + \alpha \int_\Omega |C - C^*|\ h_C\ dx. \tag{27}$$

Algorithm

From the analysis of the preceding sections we can derive the following algorithm for the minimization problem (16).

Input: initial value $C^* = C^*(x)$, applied potential $U = U(x,t)$,
measured current $i^\delta(t)$ or measured capacitance $c^\delta(t)$

(1) Solve drift-diffusion equations in thermal equilibrium (4) to obtain V_0

   (a) Solve the drift-diffusion equations (2) for C_k to obtain (V, n, p) and calculate the total current flow $\mathcal{I}$ given by (5).

   (b) Solve the linearized drift-diffusion equations (8) to obtain $(\hat{V}, \hat{n}, \hat{p})$ and the capacitance $\mathcal{C}$ given by (6).

(2) Solve (24) and or (26) for $(\lambda_1, \lambda_2, \lambda_3, \lambda_4)$.

(3) Calculate $\frac{\partial \mathcal{L}}{\partial C}(C_k)$ via (25) or (27).

(4) Determine C_{k+1} using gradient based methods.

(5) If convergence criterion is satisfied stop, else return to (1).

Both (2) and (8) are systems of time dependent partial differential equations, the computation of the solutions is quite time consuming. For the reconstruction of the doping profile one can use either current measurements and/or capacitance measurements. Using both types of measurements simultaneously requires the solution of five systems of partial differential equations, first the equilibrium solution, then the drift-diffusion equations and their linearization and finally their sensitivities. This causes a high numerical effort in the reconstruction algorithm already in the one-dimensional case.

5 Non-uniqueness of Solutions

The main focus in this section is the question whether the data determines the doping profile uniquely. In mathematical terms this question is called the identifiability, which determines whether the parameter-to-output map F is injective. Gajewski proved in [10] that for the transient drift-diffusion equations a unique solution exists. Uniqueness results were presented in the steady state case under the assumption that the applied voltage is small (see [6]).
In [6] it is shown that in one dimension the doping profile of a unipolar device can be identified uniquely from a single transient measurement. But for this result additional smoothness assumptions are required: The doping profile is assumed to be a continuously differentiable function whose partial derivatives are Hölder continuous with Hölder exponent $\alpha = 1$, i.e. $C \in C^{1,1}(\Omega)$. In case of discontinuous doping profiles these results do not apply.
So far there has been no results on the unipolar multi-dimensional inverse doping problem. For more general devices like np-diodes no uniqueness results have been derived yet.
Throughout this section only the one-dimensional case is considered and the following assumptions are made:

- The mobilities of the electrons and holes are equal, i.e. $\mu_n = \mu_p$.
- The relaxation times of the electrons and holes are equal, i.e. $\tau_n = \tau_p$.

Under these assumptions we can show that the inverse problem for the drift-diffusion equations, considering both current and capacitance measurements admits at least two solutions.

Proposition 5.1. *There exist at least two solutions $C_i \in H^1(\Omega)$, $i = 1, 2$ to the inverse problem for the drift-diffusion equations (2). In particular, if (n_1, p_1, V_1, C_1) is a solution of (2) there exists a second solution (n_2, p_2, V_2, C_2) given by*

$$C_2(x) = -C_1(1-x), \tag{28}$$
$$n_2(x,t) = p_1(1-x,t), \tag{29}$$
$$p_2(x,t) = n_1(1-x,t), \tag{30}$$
$$V_2(x,t) = -V_1(1-x,t) + U(x,t), \tag{31}$$

such that

$$J_{n_2} = J_{p_1}, \quad J_{p_2} = J_{n_1}$$
$$\mathcal{C}(V_2) = \mathcal{C}(V_1).$$

For details on the proof we refer to [11].
We consider Tikhonov regularization and obtain the minimization problem

$$Q_{\mathcal{I}}(u, C) = \left|F(C) - i^\delta(t)\right|^2 + \alpha \left|C - C^*\right|^2 \to \min_C \tag{32}$$

where $i^\delta(t)$ denotes the current measurements or

$$Q_{\mathcal{C}}(u, C) = \left|F(C) - c^\delta(t)\right|^2 + \alpha \left|C - C^*\right|^2 \to \min_C \tag{33}$$

where c^δ refers to the capacitance measurements. The operator F maps the doping profile C either to the current or to the capacitance measured at a contact Γ_1. In both cases the weak sequential closedness of F, see Proposition 3.2, ensures the existence of a solution for both minimization problems. Under the assumptions made above it has already been shown that the inverse problem admits multiple solutions, therefore one cannot expect unique minimizers of both functionals.
Indeed it is possible to construct cases where the multiple solutions are both minimizers of (32) and (33).

Proposition 5.2. *Let the assumptions of Proposition 5.1 and*

$$C^*(x) = -C^*(1-x).$$

hold. Then there exist at least two minimizers of the optimization problem (32) and (33). The multiple solutions of the inverse problem given by (5.1) are minimizers of the Tikhonov functionals (32) and (33). Furthermore

$$Q_{\mathcal{I}}(n_1, p_1, V_1, C_1) = Q_{\mathcal{I}}(n_2, p_2, V_2, C_2)$$
$$Q_{\mathcal{C}}(n_1, p_1, V_1, C_1) = Q_{\mathcal{C}}(n_2, p_2, V_2, C_2)$$

holds.

For the proof of the proposition we refer to [11]. In case of total variation regularization one can show similar results.
We mention that our analysis of multiple solutions was motivated by similar

results concerning the steady state DD-model (cf. [22]). Considering a slightly different minimization functional one could avoid the existence of the multiple solutions constructed above. This functional is given by:

$$Q_{\mathcal{I}}(u,C) = \int_0^T \left| \int_{\Gamma_1} J_n \, d\nu - i_n^\delta(t) \right|^2 dt + \int_0^T \left| \int_{\Gamma_1} J_p \, d\nu - i_p^\delta(t) \right|^2 dt + \\ + \alpha \int_\Omega \mid C - C^* \mid^2 dx. \tag{34}$$

For (34) the couple (n_2, p_2, V_2, C_2) constructed in (5.1) is not a minimizer any more. This provides reasonable remedy for optimal design and optimal control tasks as considered in [22], but for the identification of the doping profile this means that one has to measure the current caused by the holes and the current caused by the electrons separately, which is not possible in practice !

6 Numerical examples

In this section we present results of computational examples for various semiconductor devices. All computations have been performed on the software systems MATLAB 7 and FEMLAB 3.1.
In our examples we used typical parameter values of silicon and gallium arsenide at room temperature ($T = 300K$), listed in Table 1. The physical constants are listed in Table 2.
To generate artificial measurement data, we solved the direct problem (2) for an applied voltage $U = U(x,t)$ and a given doping profile $C = C(x)$ using second order Lagrange elements. This discrete data, given at certain time steps, was disturbed using the matlab function randn such that either condition (14) or (15) was satisfied. In order to avoid inverse crimes we used a different sized mesh for the evaluation of the gradient of (16) or (19).

	Physical Meaning	Silicon		Gallium Arsenide	
ϵ	permittivity	$1.0536 \cdot 10^{-12}$	$\frac{\text{As}}{\text{Vs}}$	$1.0979 \cdot 10^{-12}$	$\frac{\text{As}}{\text{Vs}}$
n_i	intrinsic carrier con.	$9.65 \cdot 10^9$	$\frac{1}{\text{cm}^3}$	$2.25 \cdot 10^6$	$\frac{1}{\text{cm}^3}$
μ_n	mobility of electrons	$1.45 \cdot 10^3$	$\frac{\text{cm}^2}{\text{Vs}}$	$9.2 \cdot 10^3$	$\frac{\text{cm}^2}{\text{Vs}}$
μ_p	mobility of holes	$0.505 \cdot 10^3$	$\frac{\text{cm}^2}{\text{Vs}}$	$0.32 \cdot 10^3$	$\frac{\text{cm}^2}{\text{Vs}}$

Table 1: Parameters of silicon and gallium arsenide at $T = 300K$

q	elementary charge	$1.6 \cdot 10^{-19}$ As
U_T	thermal voltage	0.0259 V
τ_n	lifetime of electrons	10^{-6} s
τ_p	lifetime of holes	10^{-5} s

Table 2: Physical constants at $T = 300K$

6.1 n-type Semiconductors

In this section we consider n-type semiconductors, which are obtained by adding impurities of five valence electrons to the semiconductor crystal. In this case $p = 0$ and (2) reduces to a system of two coupled PDEs. The authors are fully aware of the fact that n-type semiconductors are not used in practice by oneself, but for illustration purposes we start out with this simple example.
The predefined doping profile is $C(x) = 2x^2 - 2x + 1$, the initial guess $C^*(x) = 1$. The drift-diffusion system (2) and the sensitivities (24) are solved on a regular mesh of 330 nodes. We choose a device of length $L = 10^{-4}$ cm and a maximum doping concentration of $\tilde{C} = 10^{16}$ cm^{-3}.
The applied voltage is

$$U(x,t) = -0.5 \sin\left(\frac{\pi t}{1e5}\right).$$

For the applied time scaling we obtain

$$t = \frac{L^2}{U_T \tilde{\mu}} t_s = \frac{1e^{-8}}{1e^{-2}} t_s = 1e^{-6} s.$$

Solving the drift diffusion equations over a large time interval $\left[0 : 10^2 \ s : 10^5 \ s\right]$ seems to be a realistic setup.
Reconstructions have been performed using a projected steepest descent or a projected BFGS algorithm with the constraint

$$C(x) \geq 0.$$

The regularization parameter was chosen according to the discrepancy principle (17)

$$\delta \leq \left| F(C) - Y^\delta \right| \leq \tau \ \delta \tag{35}$$

with $\tau = 1.1$.
The reconstructed doping profile of an n-type semiconductor using a steepest descent algorithm and Tikhonov regularization is shown in Figure 1(a), for the BFGS algorithm in Figure 1(b). The steepest descent algorithm stopped after 7 iterations with $Q = 0.55$, the BFGS after 3 iteration with $Q = 0.59$. The quality of both reconstructions is approximately the same, but BFGS is faster.

6.2 Transferred-Electron Devices (TED)

A TED is the combination of a highly doped n-region, a lower doped n-region and another higher doped n-region. Material used in practice are GaAs or InP, for our example we use a TED made of GaAs of length $L = 10^{-4}$ cm and a maximum doping concentration of $\tilde{C} = 10^16$ cm^{-3}. The corresponding doping profile is given by:

$$C(x) = \begin{cases} 1 & 0 \leq x \leq 0.3 \\ 0.01 & 0.3 < x < 0.7 \\ 1 & 0.7 \leq x \leq 1. \end{cases}$$

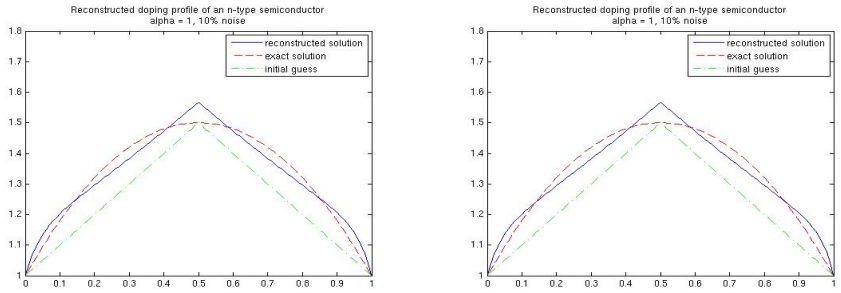

(a) Reconstructed doping profile using steep- (b) Reconstructed doping profile using BFGS est descent

Figure 1: Reconstructed doping profile using current measurements and Tikhonov regularization

We started with a good initial guess

$$C^*(x) = \begin{cases} 1 & 0 \leq x \leq 0.3 \\ 0.4 & 0.3 < x < 0.7 \\ 1 & 0.7 \leq x \leq 1. \end{cases}$$

The value of the applied potential was the same as in the case of an n-type semiconductor. Because of the two jumps we used a finer mesh with 1500 nodes. In this example we used the scaling $\mu_n = \tilde{\mu}\ \mu_{n_s}$. This results in a different time scale

$$t = \frac{L^2}{U_T \tilde{\mu}} t_s = \frac{1e^{-8}}{1e^{-2}1e^{3}} t_s = 1e^{-9} s.$$

Therefore we solved the system on the interval $\left[0 : 10^4 : 10^7\right]$.

Current Measurements:
After three iterations the reconstruction stopped because the calculated gradient yielded no descent direction. Figure 2(a) shows the reconstructed doping profile after 3 iterations, Figure 2(b) the gradient evaluation for this doping profile.

Capacitance Measurements:
In the case of capacitance measurements such issues do not occur. The parameters are the same as in the case of current measurements. The reconstruction from capacitance measurements is more time consuming than in case of current measurements due to the numerical integration of the right hand side of equation (26b). The reconstructed doping profile can be seen in Figure 3. When using Tikhonov regularization the solution becomes smoother - this can be seen in this example.

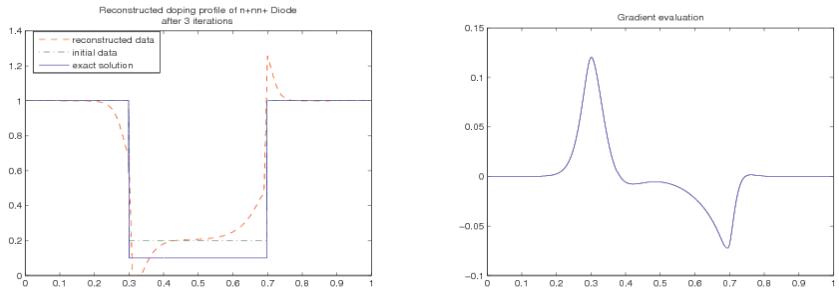

(a) Reconstructed doping profile

(b) Gradient after 3 iterations

Figure 2: Reconstructed doping profile after 3 iterations using current measurements

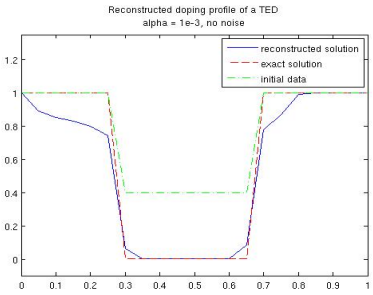

Figure 3: Reconstructed doping profile using capacitance measurements

6.3 np-Diodes

In this section we present numerical examples, which illustrate the difficulties that arise due to the non-uniqueness of the regularized solution. We used a mesh of 1100 nodes to generate data and 1050 nodes to evaluate the gradient of the minimization functional.
We consider a semiconductor device of length $L = 10^{-4}$ cm and a maximum doping concentration $\tilde{C} = 10^{16}$ cm^{-3}. Setting $\tau_n = \tau_p = 1e^{-6}$ and $\mu_n = \mu_p = 1000$ allows the existence of multiple solutions as described in Section 5.
The exact doping profile is given by

$$C(x) = \begin{cases} 1 & 0 \leq x \leq 0.5 \\ -0.5 & 0.5 < x \leq 1 \end{cases}$$

the initial guess by

$$C^*(x) = \begin{cases} 1 & 0 \leq x \leq 0.5 \\ -0.3 & 0.5 < x \leq 1. \end{cases}$$

In Figure 4(a) the two possible solutions that produce the same total current are illustrated. In Figure 4(b) the gradient of the initial guess is shown - this gradient would be a steepest descent direction for the second solution, but not for the first one.
In the second example we set $\mu_n = 1500$ and $\mu_p = 450$. Furthermore when considering the symmetric doping profile

$$C(x) = \begin{cases} 1 & 0 \leq x \leq 0.5 \\ -1 & 0.5 < x \leq 1 \end{cases} \tag{36}$$

the two possible solutions are identical. We solve the problem over the time interval $\left[0 : 10^2 s : 10^5 s\right]$. The applied voltage is given by

$$U(x,t) = 0.5 \sin\left(\frac{\pi t}{1e^5}\right).$$

To create artificial data we solved the drift-diffusion equations for the doping profile (36) and added 10% noise to the current. This data is used as an input for the reconstruction of the doping profile and can be seen in Figure 5. Note that the computed artificial data is not smooth at the interval $\left[2.5 \cdot 1e^4, 3 \cdot 1e^4\right]$, which has an effect on the quality of the reconstructed doping profile.

For this problem setup we reconstructed the doping profile using Tikhonov

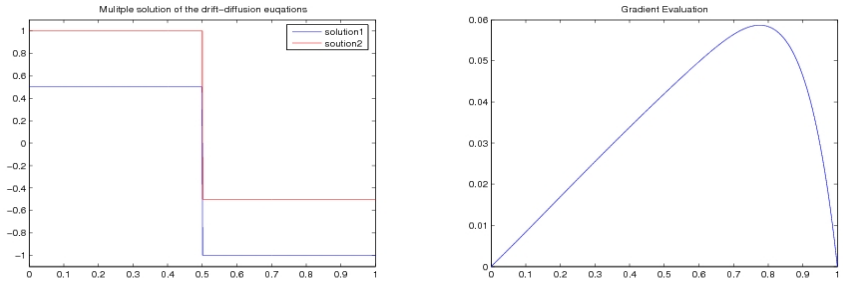

(a) Possible multiple solutions (b) Gradient Evaluation

Figure 4: Multiple solution in case of a np-diode

and total variation regularization. The reconstructed solution using Tikhonov regularization and the corresponding cost functional is displayed in Figure 6. In case of total variation regularization the solution and the corresponding doping profile are displayed in Figure 7. Note that the jump of the regularized solution using total variation regularization is much steeper than in case of Tikhonov regularization.

References

[1] W.R. van Roosbroeck. Theory of the flow of electrons and holes in germanium and other semiconductors. *Bell System Technical Journal*, pages 560–607, 1950.

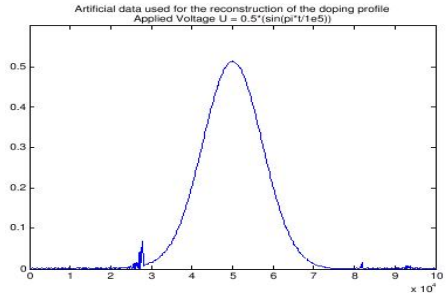

Figure 5: Reconstructed doping profile using current measurements

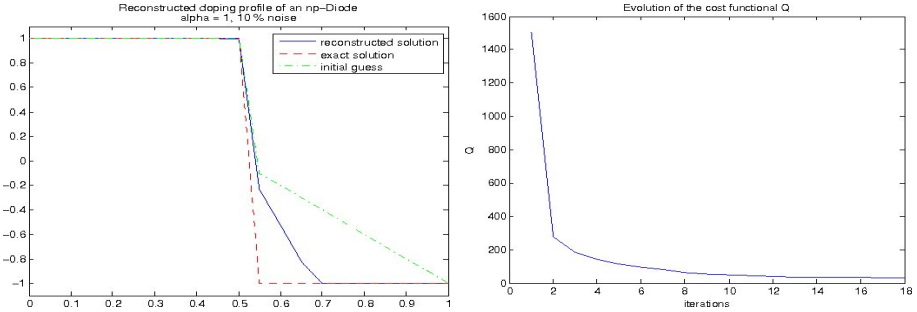

(a) Reconstructed doping profile (b) Evaluation of the cost functional Q

Figure 6: Reconstructed doping profile using current measurements

[2] P. A. Markowich. *The stationary semiconductor device equations*. Computational Microelectronics. Springer-Verlag, Vienna, 1986.

[3] P. A. Markowich, C. A. Ringhofer, and C. Schmeiser. *Semiconductor equations*. Springer-Verlag, Vienna, 1990.

[4] M. Hinze and R. Pinnau. An optimal control approach to semiconductor design. *Math. Models Methods Appl. Sci.*, 12(1):89–107, 2002.

[5] M. Burger and R. Pinnau. Fast optimal design of semiconductor devices. *SIAM J. Appl. Math.*, 64(1):108–126 (electronic), 2003.

[6] M. Burger, H. W. Engl, and P. A. Markowich. Inverse doping problems for semiconductor devices. In *Recent progress in computational and applied PDEs (Zhangjiajie, 2001)*, pages 39–53. Kluwer/Plenum, New York, 2002.

[7] M. Burger, H. W. Engl, P. A. Markowich, and P. Pietra. Identification of doping profiles in semiconductor devices. *Inverse Problems*, 17(6):1765–1795, 2001.

[8] M. Burger, H. W. Engl, A. Leitao, and P. A. Markowich. On inverse problems for semiconductor equations. *Milan J. Math.*, 72:273–313, 2004.

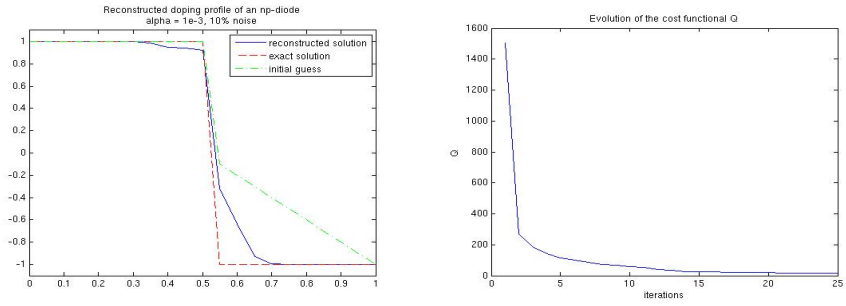

(a) Reconstructed doping profile (b) Evaluation of the cost functional Q

Figure 7: Reconstructed doping profile using current measurements

[9] W. Fang and K. Ito. Reconstruction of semiconductor doping profile from laser-beam-induced current image. *SIAM J. Appl. Math.*, 54(4):1067–1082, 1994.

[10] H. Gajewski. On existence, uniqueness and asymptotic behavior of solutions of the basic equations for carrier transport in semiconductors. *Z. Angew. Math. Mech.*, 65(2):101–108, 1985.

[11] M.-T. Wolfram. Semiconductor inverse dopant profiling from transient measurements. Master's thesis, Johannes Kepler University Linz, 2005.

[12] P. A. Markowich and Ch. A. Ringhofer. Stability of the linearized transient semiconductor device equations. *Z. Angew. Math. Mech.*, 67(7):319–332, 1987.

[13] D. K. Schroder. *Semiconductor material and device charcterization, 2nd edition*. John Wiley & Sons, Inc., 1998.

[14] H. W. Engl, M. Hanke, and A. Neubauer. *Regularization of inverse problems*, volume 375 of *Mathematics and its Applications*. Kluwer Academic Publishers Group, Dordrecht, 1996.

[15] Victor Isakov. *Inverse problems for partial differential equations*, volume 127 of *Applied Mathematical Sciences*. Springer, New York, second edition, 2006.

[16] L. Rudin, S. Osher, and E. Fatemi. Nonlinear total variation based noise removal algorithms. *Physica D: Nonlinear Phenomena*, (60):259–268, 1992.

[17] D. Dobson and O. Scherzer. Analysis of regularized total variation penalty methods for denoising. *Inverse Problems*, 12(5):601–617, 1996.

[18] R. Acar and C. R. Vogel. Analysis of bounded variation penalty methods for ill-posed problems. *Inverse Problems*, 10(6):1217–1229, 1994.

[19] M. B. Giles and N. A. Pierce. An introduction to the adjoint approach to design. *Flow, Turbulence and Combustion*, 65:393–415, 2000.

[20] P. E. Gill, W. Murray, and M. H. Wright. *Practical optimization*. Academic Press Inc. [Harcourt Brace Jovanovich Publishers], London, 1981.

[21] R. Fletcher. *Practical methods of optimization*. Wiley-Interscience [John Wiley & Sons], New York, second edition, 2001.

[22] M. Hinze and R. Pinnau. Multiple solutions to a semiconductor design problem. Technical Report Preprint MATH-NM-14-2003, TU Dresden, 2005.